

# **A micro mechanical study on failure initiation of dual phase steels under tension using single crystal plasticity model**

J. Kadkhodapour<sup>1\*</sup>, A. Butz<sup>3</sup>, S. Ziaei-Rad<sup>1</sup>, S. Schmauder<sup>2</sup>,

<sup>1</sup> Mechanical Engineering Department, Isfahan University of Technology, Isfahan 84156-83111, Iran

<sup>2</sup> Institut für Materialprüfung, Werkstoffkunde und Festigkeitslehre (IMWF), University of Stuttgart, Germany

<sup>3</sup> Fraunhofer-Institute for Mechanics of Materials IWM, 79108 Freiburg, Germany

## **Abstract**

Both experimental and numerical methods were employed to investigate the mechanism of failure in dual phase steels. The tensile test was interrupted in different steps to capture the mechanism of void initiation and void growth during material failure. The results can be considered as a first report for the commercial DP800 steel. Numerical simulations, which were carried out using the real micro-structure, are able to predict the void initiation in the material. In addition, through the numerical simulation a new understanding of the deformation localization was gained. Deformation localization, which causes severely deformed regions in the material, is most probably the main source of rupture in the final stages of the failure. In the SEM micrographs of the material after failure some voids are observable which can validate the results obtained by the simulation.

**Keywords:** Dual Phase (DP) Steel, Failure Mechanism, Tensile Test, Crystal plasticity based finite element method (CPFEM), Microstructural modeling, Localized deformation, Void initiation, Real Microstructure.

---

\* Contact Author: J.Kadkhodapour, Department of Mechanical Engineering, Isfahan University of Technology, 84156, Isfahan, Iran  
Email: [kadkhodapour@me.iut.ac.ir](mailto:kadkhodapour@me.iut.ac.ir)

## **1. Introduction**

Dual phase steels are among the most important advanced high strength steel (AHSS) products recently developed for the automotive industry. This group of steels is very interesting for light weight constructions because it combines a high ultimate strength with a high fracture strain. On the market, DP 800 steels with an ultimate strength of 800 MPa and a nominal fracture strain of approximately 20% are available. Another advantage of this material is its low yield strength, high hardening ratio and absence of discontinuous yielding. For this reason dual phase steel sheets are well suited for forming and deep drawing processes.

The microstructure of dual phase steels typically consists of a soft ferrite phase with dispersed islands of a hard martensite phase. The harder martensite grains explain the high strength of these material in terms of a composite effect on yield stress and work hardening (Bouaziz (2007), Kumar (2008)). Despite many simplifications; the composite model is able to describe the material hardening with quite good accuracy. To investigate the problem of failure the microstructure of the material has to be described and considered more accurately. There exist three kinds of other phases in the ferrite matrix: (1) large ( $>4\mu\text{m}$ ) martensite grain, (2) medium (between  $1\mu\text{m}$  and  $2\mu\text{m}$ ) ceramic inclusions of aluminum-oxide or manganese-sulfide and (3) small (nano scale) carbide particles. While carbide particles contribute to the strength of material by impeding the motion of dislocations, the ceramic inclusions exist in the material as undesirable relics from production process or from raw materials. The martensite phase is an essential component of DP steels to increase the strength of material. The effects of these three phases have to be considered in describing the failure mechanism of dual phase steels.

### **1- Mechanism of failure in dual phase steels**

- **Damage failure**

Damage mechanisms are classically used to explain the failure mechanism in metals and more specifically in steel. For ferritic steel, in which the martensite grains do not exist, the process of failure is explained in the following way. Ceramic inclusions are often weakly bonded and initiate voids easily. As these voids grow, straining of the inter-void material becomes intense, which eventually leads to breakage or decohesion of the strong and well bonded carbide particles. However, in modern steels the volume fraction of ceramic inclusions has decreased significantly so that their effect on the final failure is considered to be very low (Riedel (1992)).

In order to explain the failure of dual phase steels by a damage mechanism, researchers considered the martensite grains as the site of the void initiation. It is believed by many authors that the brittleness of the martensite phase is likely to promote damage (Shen (1986), Kang (2007), Uthaisangsuk (2008, 2009)). Damage slightly reduces the global mechanical properties, but more importantly it reduces the ductility, and this is probably now the main limitation to further improvements in the performance of dual phase steels. Many investigators like (Rashid (1977), Rashid (1978), Balliger (1982)) have observed that void formation arises from both martensite particle fracture and interface decohesion. (Balliger (1982), Gladman (1997), Koo (1977)) stressed that major voids form in the fracture of martensite particles. (Sun (2002)) have observed that the formation of voids takes place by both mechanisms depending on the morphology of the martensite. (Steinbrunner (1988)) observed three mechanisms of void formation, namely, interface decohesion, martensite fracture, and uniquely identified martensite separation. (Kang (1987)) studied the fracture behavior of intercritically treated structure in medium carbon steels and observed that the ferrite–martensite interface decohesion was the predominant mode of void nucleation and growth, where martensite structure was of the lath type. Other researchers such as (Gerbase (1979), Speich (1979), Korzekwa (1980), Szewczyk (1982)) have reported that void

formation occurs due to martensite–ferrite interface decohesion. (Szewczyk (1982)) have not observed any particle cracking for martensite volume percent ( $V_m$ ) in the range 15–20%.

Nam (1999) have shown that unlike martensite particles aligned nearly parallel to the drawing axis, which are thinned to fibrous shape, those aligned transverse to the drawing axis are severely bent and even fractured with increasing longitudinal strain. They stated that the majority of voids which lead to fracture are formed at the ferrite–martensite interface, rather than the cracked martensite, and eventually coalesce to cause failure during subsequent tensile loading or drawing. Ahmed (2000) have identified three modes of void nucleation, namely martensite cracking, ferrite–martensite interface decohesion, and decohesion at the ferrite–ferrite interfaces with minimum plastic deformation. They reported that at low to intermediate  $V_m$ , the void formation was due to ferrite–martensite interface decohesion, while the other two mechanisms are most probable to occur at high  $V_m$  (above 32%).

Most recently, Maire (2008) carried out in situ tensile tests on a dual-phase steel specimen. In addition, using X-ray tomography he followed and quantified the evolution of damage nondestructively in three dimensions. He concluded from micrographs and through other types of observation that damage is never observed in the ferrite phase. Also he observed both martensitic fracture and ferrite/martensite decohesion during the test. By X-ray topography, he carried out some measurements on the process of void initiation and void growth in the material. The information from X-ray topography was then used to develop a new model for void growth based on the classical Rice and Tracey (1969) approach.

- **Failure due to other factors**

In many research works, the failure of dual phase steels is explained through a rather simple damage mechanism (described before as void initiation around or inside martensite grains and

growth and coalescence of voids due to ferrite failure). There are also some investigations that do not support this idea.

In ferritic structural steels, void nucleation has been identified with two types of second phase particles—non-metallic inclusions (Spitzig (1988), Qiu (1999)) and carbides (LeRoy (1981), Kwon (1988)). The strain of void nucleation and the interface strength for these two second phase particles are frequently reported in literature (Qiu (1999), LeRoy (1981), Kwon (1988), Kosco (1993)). Poruks (2006) used the same method to measure the value of nucleation strain for martensite particles. From the results of these works, it can be concluded that the experimentally determined void nucleation strain and the calculated interface strength ( $\sigma_f$ ) increases in the following order: non-metallic inclusion ( $\sigma_f \approx 1.1\text{-}1.4$  GPa) , carbide particles ( $\sigma_f \approx 1.2\text{-}2.0$  GPa), and martensite grains ( $\sigma_f \approx 2.4\text{-}2.5$  GPa). This is consistent with what is known about the structure of the interfaces for these various dispersed phases. The low void-nucleation strains for non-metallic inclusions arise from pre-existing cracks and weakly bonded interfaces (Poruks (2006)).  $\text{Fe}_3\text{C}$  particles form by solid-state transformation and often have faceted interfaces, which is indicative of semi-coherent interfaces. The high strength of the ferrite/martensite interface is explained by Lee (2004) in the following way. The carbon atoms are diffused from martensite to ferrite when the martensite phase is decomposed during tempering process. This carbon diffusion reinforces the ferritic matrix near the ferrite/martensite interface and increases the interfacial strength between ferrite and martensite. Considering a higher strength for the region near the ferrite-martensite interface raises some questions about the validity of the idea of void initiation and growth in this region.

Some investigations on simple tension tests were carried out by Tasan et al. (2009) on dual phase steels. After each tension test, they did indentation tests on the cross section of their specimen. They expected to observe a sudden drop in the hardness curve due to the damage near the failure surface. However, no noticeable drop in either nanohardness or microhardness

was observed. They relate this phenomenon partly due to other mechanisms that are acting in parallel to the simple damage mechanism, such as strain hardening, grain shape change, texture development, residual stress and indentation pile-up.

Based on the above observations, one can claim that as the hardness is not only due to damage, failure can also be affected by several other mechanisms in addition to damage. One of these mechanisms which attract the researchers who are working in this field is shear banding and strain localization.

- **Shear banding and localization**

The local deformation field and its effect on the failure pattern was the subject of many works. Even though dual phase steels exhibit a macroscopically uniform and homogenous deformation mode, from a micromechanical perspective, its plastic deformation is inherently inhomogeneous due to its nature of the grain level inhomogeneity. Shen (1986) used a scanning electron microscope (SEM) equipped with a tensile straining stage to illustrate the inhomogeneous strain distributions between the ferrite and martensite grains in DP steels. They observed that, in general, the ferrite phase deformed immediately and at a much higher rate than the delayed deformation of the martensite phase. For DP steels with low martensite volume fraction, only the ferrite deforms and no measurable strain occurs in the martensite particles; for dual phase steels with high martensite volume fraction, shearing of the ferrite-martensite interface occurs extending the deformation into the martensite islands. More recently, Kang (2007) used the digital image correlation method to measure the microscopic strain distribution and damage in DP steels at the grain level. It is found that the strain heterogeneity in areas that contain ferrite constrained by martensite is much higher than in other areas, and that heat treatment changes the microscopic strain distribution at the grain level and thus affects the tensile properties of the materials. Localized deformation due to

stiffness mismatch as a special distinctive void nucleation mechanism was studied by Erdogan (2002) and Steinbrunner (1988). Steinbrunner (1988) observed that the nucleation of voids due to localized deformation within the martensite or by martensite particle separation may be more complex than previously thought. He mentioned that as a consequence of localized neck formation, strain localization in the form of shear bands can develop to further concentrate flow to failure. Kim (1981) describes the failure process of dual phase steels as follows. Because the flow strength of ferrite is much lower than that of martensite, plastic deformation begins in the soft ferrite while the martensite is still elastic. This plastic deformation in the ferrite phase is constrained by the adjacent martensite, giving rise to a build-up of stress concentration in the ferrite. Thus the localized deformation and/or stress concentration in the ferrite lead to fracture of the ferrite matrix which occurs by cleavage or void nucleation and coalescence depending of the morphological difference. The in situ SEM observation of Suh (1997) shows that micro-fracture occurs in the severely deformed region of the ferrite matrix rather than at the martensite particles. It is mentioned that this is mainly due to the lower yield strength of ferrite and higher localized strain in that region.

Tomota (1982) presents pictures of the deformation fields in different DP steels. He reports that the degree of inhomogeneity of plastic deformation is extremely influenced by three factors: volume fraction of the martensite phase, the yield stress ratio of the ferrite-martensite phases and the shape of the martensite phase. Tomota also measured the residual stress by X-ray stress analysis on the surface and suggests that each constituent phase deforms under a multiaxial stress condition.

## **2- Simulation of tensile behavior and failure in multiphase material**

In the studies of ductile failure, finite element models which are based on classical micromechanical considerations (Gurson (1977)) are typically used. The voids or harder phases are usually assumed to be cylindrical or spherical inclusions, and final ductile failure

can be predicted as a sequence of void nucleation, growth and coalescence (Orsini (2001), Al-Abbasi (2007), McVeigh (2007))

Recently, Sun et al. (Sun (2009a), Sun (2009b)) developed a microstructure-based modeling procedure in which the failure mode and ultimate ductility of dual phase steels are predicted under different loading conditions using the plastic strain localization theory. For DP980 and DP780, Sun et. al demonstrated that microstructure-level inhomogeneity of the steels can serve as the initial imperfections triggering the instability which induces plastic strain localization during deformation process. No pre-existing micro-voids need to be introduced in the microstructure, and no prescribed failure criterion is necessary in predicting plastic strain localization in the model. Ductile failure is predicted as the natural outcome of the plastic strain localization due to the incompatible deformation between the hard martensite phase and the soft ferrite phase. These results indicate that for DP980 and DP780, microstructure-level inhomogeneous strain distribution during deformation may be the key factor influencing the ductility of these steels. The driving force for ductile fracture in these steels may no longer be just void growth and coalescence but also strain localization between the ferrite and martensite phase. It is claimed by Sun (Sun (2009a), Sun (2009b)) that this consideration agrees with the experimentally observed failure mechanism.

In addition to the above mentioned works which simulate the final failure of material, several studies focused on the investigation of void initiation in microstructures. Actually, having access to the variation of the strain and stress fields on the microscale can help to understand the plastic deformation and the failure initiation process. A number of investigations are devoted to the examination of stress and strain localization at the microscale. The works of Barbe (2001), Diard (2005), Nakamachi (2000) and Marketz (2003) provide good examples of this approach.



***Crystal Plasticity:*** Micro-mechanical modeling within the framework of crystal plasticity has been extensively employed in simulating the mechanical response of materials (Anand (1994), Prakash (2009), Bieler (2009)). The macroscopic material behavior, as well as the evolution of field quantities at the microscopic level, can be numerically calculated and clarified by considering the micro-structural features of the grains. In crystal plasticity analyses, each grain is associated with different crystallographic orientations so the development of deformation texture and possible flow localization can be predicted.

The Crystal Plasticity Finite Element Method (CPFEM) has now become a regular tool for studying the microscopic heterogeneity associated with the plastic deformation in metals. Several works investigated the evolution of the heterogeneous strain field throughout a plastically deforming microstructure (K-Kanjarla (2008), Diard (2005), Delannay (2008), Osipov (2008)). Also, some investigations have been carried out by CPFEM and the results were compared with experimental observations (Ma (2006a,b), Zaafarani (2006)). Recently some publications devoted to modeling of site-specific stress-strain histories with crystal plasticity finite element modeling of representative microstructural volumes and characterizing the damage nucleation events microscopically (Bieler (2009)).

The current work is concentrates on the pure and low grain size DP steel. While in the old generation of DP steels, a high volume percent of inclusions and large grains sizes were observed, the current material shows a low volume percent of inclusion and a small grain size. The results of this investigation show that the mechanism of failure changes significantly due to the change in these two parameters. The results of Calcagnotto (2010) from investigation of failure of dual phase steel with different grain sizes show that while in classical DP steels (of coarse grain and high impurity) the cleavage fracture and grain split cause failure, in modern DP steels (of fine grain and low impurity) grain boundaries play the significant role. The current work extensively investigates the underlying mechanism of grain boundary failure in modern DP steels.

Recently, failure mechanism in modern dual phase steels is a subject of interest for several research groups (Sun(2009), Avramovic (2009a), Uthaisangsuk (2009), Calcagnotto (2010)). They approach the problem through different scientific methods. The current work tries to carry out both experiments and simulations in micro scale. The results and the approach seem to be an improvement in the current state of art in study of failure in heterogeneous material. Using the simulation results, the material behavior is discussed in details and the suggested mechanism seems to give a deeper understanding about the mechanism of failure in dual phase steels.

Methodologically, the work tries to use both experimental and simulation procedures, and to improve upon recent simulation works in this field (Sun (2009a), Sun (2009b)) by introducing the crystal plasticity and texture into the model, and to simulate experimental results on a micro scale which can be comparable with simulation. The experimental method which had previously been used in other investigations (Avramovic (2009a), Avramovic(2009b)) and carried out here with some modification to get more accurate results for this special material.

## 2. Experimental Procedure and Results

A commercial high-strength dual phase DP800 steel was studied in the present work. Rolled sheet was manufactured in the SZAG company for this research project. It was received in the form of 1.75mm thick sheets. The tensile specimens were machined in such a way that the applied tensile loading axis corresponded to the rolling direction (RD) of the sheet. The gage length of specimen was 2.5mm and tensile testing was performed at a crosshead speed of 0.615µm/s on a servo-hydraulic standard testing machine.

The engineering stress–strain curves of the analyzed DP800 steel obtained from the uniaxial tensile test is given in Fig 1. The load was applied in rolling direction. This steel is characterized by very uniform plastic flow until necking.

Fig 2 shows the microstructure of the analyzed DP800 material, which was provided by the steel company. The micrograph shows a through-thickness cross-section of the central part of the sheet comprising a ferrite matrix and martensite second phase. It is seen that the spatial distribution of martensite is not uniform: the microstructure exhibits martensite banding in lines parallel to the rolling plane. These lines originate from the former pearlite bands of the cold rolled sheet. The volume fraction of 23% was determined for the martensite phase. An average grain size of approximately 6µm was obtained for the ferrite phase.

To exactly analyze the process of void nucleation and growth, the tests were carried out on three specimens. For the first specimen the tensile test was interrupted after diffuse necking ( $\epsilon_{\text{eng}} \approx 0.12$  in the first row of Fig 3). The second one was interrupted right before failure ( $\epsilon_{\text{eng}} \approx 0.17$  in the second row of Fig 3), and finally the third specimen was tested until failure ( $\epsilon_{\text{eng}} \approx 0.20$  in the third row of Fig 3). Light microscopy and SEM analyses were carried out for all three specimens.

Metallographic analysis of damage accumulated along the gauge length after uniaxial tensile testing was carried out on deformed and failed samples, on cross-sections along the tensile axis. Tensile specimens were sectioned through-thickness along the mid-width in longitudinal direction. To preserve any damage during specimen preparation, wire electrical discharge machining (WEDM) was used for the cutting process. The SEM analysis of void nucleation mechanisms were carried out on the same samples. In addition, pictures of light microscopy were taken from specimens to exactly clarify the microstructure.

Figs 3a-d show some detailed inspection of voids initiation. Fig 3a shows the specimen which is deformed to the diffuse necking point and Fig. 3b, c, d are the SEM images from a section of that specimen. Fig 3b shows that some of the voids are nucleated in the ferrite-ferrite grain boundaries. This type of void initiation seems to take place always in the direct neighborhood of a martensite particle. Thus, stress concentration or deformation mismatch might be a reason. In ferrite-martensite grain boundary two patterns of void initiation can be observed. The first pattern which is shown by arrow in Fig 3c is similar to crack propagation. It seems that in this region the initial void forms in ferrite-ferrite grain boundary and then propagates to the ferrite-martensite grain boundary like a crack. The second pattern, which is indicated by the rectangle in Fig 3c and magnified in Fig 3d, can be named normal separation of ferrite/martensite grain boundary.

Figs 3e-h show some detailed inspection of voids growth. In this stage, the specimen is under localized necking as can be observed in Fig 3e and Fig. 3f, g, h are the SEM images from a section of that specimen. In the observed central region, Figs 3f, g, most of the voids extends in tensile direction and in the boundary of ferrite grains. Voids will also grow if they are situated between two closely spaced martensite grains. They can be considered as the voids around martensite particle but they originate from ferrite-ferrite grain boundary separation. Even these voids can propagate as a crack in ferrite-martensite grain boundary. Fig 3h shows two voids which grow around inclusions. Only a small number of inclusions were found in

the complete analysis. Therefore, it is not expected that they play an important role for the main failure mechanism. Fracture of martensite particles may contribute to void initiation but this could not often be observed.

The patterns of voids for a broken specimen are shown in Fig 3i-l. The failed specimen can be observed in Fig 3i and Fig. 3j, k, l are the SEM images from a section of that specimen. In the central region the normal ductile fracture pattern can be observed (Fig 3j) but away from the center shear fracture is dominant (Fig 3i). A new kind of voids can be observed in the failed part (Fig 3l). These voids can be named as shear type voids or rupture voids.

It was mentioned before that the current steel is considered to be a very pure dual phase steel. The steel producer claims that there is a low volume percent of inclusion in the current steel. The fractography results in Fig. 4a show that the voids have a homogeneous pattern and large extensive voids cannot be observed so often. Also from Fig. 4b it can be observed that the ceramic inclusions are not present at the bottom of voids.

### **3. Micromechanical Simulation**

#### **3.1. Generation of Micromechanical Model for Material**

To generate the model of the DP 800 microstructure shown in Fig. 5a, the image is first automatically segmented into two different phases using photo-processing software Corel Draw. The segmentation is done by adjusting contrast and colors such that all martensite grains end up black while all ferrite grains end up white. It can be observed in Fig. 5b. In Fig 5c, the ferrite matrix is divided into 250 grains of different orientations. The orientation of grains is assigned in a way that real texture (Fig. 5c) was considered for the material.

Crystallographic texture is quantified by the orientation distribution function (ODF) which defines the probability that a volume fraction of the polycrystalline aggregate is taken up by crystallites of special orientation. Experimentally, an ODF is accessible either directly from electron backscatter diffraction (EBSD) data on a large number of (surface) grains or by calculation from X-ray or neutron diffraction based pole figures. In this work, the real texture which was measured by neutron diffraction based pole figures was assigned to 250 separate grains. The theoretical background of this process can be found in Eisenlohr (2008).

The meshing of the microstructure and assigning orientation to the grains was carried out simultaneously with the division of ferrite matrix into separate grains. On the other hand, comparing Fig. 5a, d shows that the exact grain shape of ferrite matrix was not considered in this study but it was divided in a way that the approximate grain size in model and real microstructure would be the same. The idea behind modeling of material was that the inhomogeneity due to microstructure and grain inhomogeneity should be modeled exactly.

### 3.2. Crystal plasticity model for ferrite phase

Shear-banding is a consequence of the correlation of microscopic plastic events. At the atomic level the most elementary shear events occur at kinks along dislocation lines. On the other hand, on grain scale, it happens due to crystalline slip in activated slip systems. In this sense, the crystal plasticity constitutive law is applied for modeling of shear localization in the microscopic simulation. In addition crystal plasticity gives the opportunity to study the texture effect in the microstructural model.

Single crystal plasticity theory (Asaro (1983a), Asaro (1983b)) is based on the assumption that plastic deformation is the sum of the crystalline slip in all activated slip systems. Schmidt (Schmidt (1931)) pointed out that plastic slip occurs when the resolved shear stress onto a crystallographic plane in the direction of slip reaches a critical value. The precise theory was formulated by Rice (1971) and Hill (1972). The commercially available finite element software ABAQUS in combination with a user material subroutine based on the work of Huang was used for the finite element simulations. The essential relations of the constitutive model are summarized as follows. A more detailed description can be found in (Huang (1991)).

The resolved shear stress  $\tau^{(\alpha)}$ , on the  $\alpha$ -th slip system is computed from the stress tensor  $\sigma_{ij}$  as:

$$\tau^{(\alpha)} = \sigma_{ij} \mu_{ij}^{(\alpha)} \quad (1)$$

With  $\mu_{ij}^{(\alpha)}$  being the Schmidt tensor given by

$$\mu_{ij}^{(\alpha)} = \frac{1}{2} (s_i^{(\alpha)} n_j^{(\alpha)} + s_j^{(\alpha)} n_i^{(\alpha)}) \quad (2)$$

Where  $\underline{s}^{(\alpha)}$  is the vector tangent to slip system  $\alpha$  and  $\underline{n}^{(\alpha)}$  is the vector normal to slip system  $\alpha$ .

The plastic strain rate is given by

$$\dot{\epsilon}_{kl}^p = \sum_{\alpha} \mu_{ij}^{(\alpha)} \dot{\gamma}^{(\alpha)} \quad (3)$$

The shear strain rate in slip system  $\alpha$  is  $\dot{\gamma}^{(\alpha)}$ . The stress rate is then defined as

$$\dot{\sigma}_{ij} = C_{ijkl} \dot{\epsilon}_{kl}^e = C_{ijkl} (\dot{\epsilon}_{kl} - \dot{\epsilon}_{kl}^p) \quad (4)$$

$\dot{\epsilon}^e$  and  $\dot{\epsilon}^p$  represent elastic and plastic strain respectively. A viscoplastic constitutive model is used in this study in the form of a power law expression as

$$\dot{\gamma}^{(\alpha)} = \dot{\gamma}_0^{(\alpha)} \operatorname{sgn}(\tau^{(\alpha)}) \left| \frac{\tau^{(\alpha)}}{g^{(\alpha)}} \right|^{1/n} \quad (5)$$

where  $g^{(\alpha)}$  is the current strength of each slip system  $\alpha$ ,  $\gamma_0$  is the reference (initial) shear strain, while  $n$  is the strain rate sensitivity parameter. A larger value of  $n$  ensures the rate independent case, such as  $n=50$ . As  $n \rightarrow \infty$ , the plastic constitutive formulation formally becomes rate-independent. The strain hardening is defined as follows:

$$\dot{g}^{(\alpha)} = \frac{d\hat{\tau}^{(\alpha)}}{d\Gamma} \sum_{\beta} h_{\alpha\beta} \dot{\gamma}^{(\beta)} \quad (6)$$

The diagonal elements of the hardening matrix  $h_{\alpha\beta}$  describe self hardening, and off-diagonal elements describe latent hardening. The hardening function  $\hat{\tau}^{(\alpha)}$  is formulated as a modified Voce law and defined as:

$$\hat{\tau}^{\alpha} = \tau_0^{\alpha} + (\tau_1^{\alpha} + \theta_1^{\alpha} \Gamma) \left( 1 - \exp\left(-\frac{\theta_0^{\alpha} \Gamma}{\tau_1^{\alpha}}\right) \right) \quad (7)$$

where  $\tau_0^{\alpha}, \tau_1^{\alpha}, \theta_0^{\alpha}, \theta_1^{\alpha}$  are the hardening parameters and  $\Gamma$  is the cumulative shear on all slip systems.

The stress and strain field of the micromechanical model for each time increment is



numerically homogenized in order to obtain macroscopic stress-strain response.

### 3.3. Material behavior

In dual phase steels, the coupled combination of chemical composition and processing conditions allows to produce a broad range of microstructures leading to significantly different mechanical behavior in steels. Several works have been published about accurate measurement of mechanical properties in each phase (Sun (2009a, b) and Rodriguez(2004)).

Rodriguez (2004) carried out nanohardness test to estimate the accuracy of predictions obtained from an empirical model formulation. As the accuracy of the results seems to be satisfactory, this method is used in this study to estimate the stress-strain relation of the single phases. Following (Rodriguez (2004)), the stress-strain relation is given by

$$\sigma = \sigma_0 + \Delta\sigma + \alpha \cdot M \cdot \mu \cdot \sqrt{\frac{1 - \exp(-M \cdot k \cdot \varepsilon^p)}{k \cdot L}} \quad (8)$$

$$\sigma_0 = 77 + 80\% Mn + 750\% P + 60\% Si + 80\% Cu + 45\% Ni + 60\% Cr + 11\% Mo + 5000 N_{ss} \quad (9)$$

In this equation,  $\alpha$  is a constant ( $\alpha = 0.33$ ),  $M$  is taylor factor ( $M = 3$ ),  $\mu$  is the value of shear modulus ( $\mu = 80000\text{MPa}$ ) and  $b$  is the value of Burger's vector ( $b=2.5 \times 10^{-10}$  m).  $L$  is the dislocation mean free path,  $k$  is the indication of the recovery rate and  $\varepsilon^p$  is the plastic strain.  $\Delta\sigma$  is the additional strengthening due to the precipitation and carbon in solution. The value of  $\sigma_0$  takes into account the effect of Pierls stress and of the elements in solid solution. The values of  $L$ ,  $k$ ,  $\Delta\sigma$  are assigned to be  $5\text{E-}6$ ,  $2$ , and  $100$  respectively for ferrite and  $3.8\text{E-}8$ ,  $41$ ,  $1500$  respectively for martensite according to studies by Rodriguez (2004).

Based on these relations and the chemical data, which were collected from this special steel, the stress strain curve for ferrite of  $0.02\%$  carbon content and  $5\mu\text{m}$  grain diameter and also martensite of  $0.64\%$  carbon content are plotted in Fig 7.

For the martensite phase, the elasto-plastic material behavior is considered. An isotropic hardening law is assigned for the plastic state. The yield stress is given as a tabular function of plastic strain according to Fig. 7 and Rodriguez (2004) calculations. But for the ferrite grains the crystal plasticity constitutive law will be used. The constants for crystal plasticity law will be calculated in Section 6.1.

### 3.4. Boundary conditions and mesh

Periodic boundary condition results in the periodic deformation of the micromechanical model, i.e. a bump on one side of the micromechanical model corresponds to an indent at the opposite site. The boundary condition for micromechanical model was assigned in the following way. Essentially, two equivalent points a and b, located on opposite sides of the unit cell, are coupled with the macroscopic deformation gradient.

$$u_i^b - u_i^a = \bar{F}_{ij}(x_{j0}^b - x_{j0}^a) - (x_{i0}^b - x_{i0}^a) \quad (10)$$

Where  $x_{i0}^a$ ,  $x_{i0}^b$  indicate the position of a point pair in the non-deformed configuration. It is noted that periodic boundary conditions minimize constraint effect. The periodic boundary condition was applied in X, Y and Z direction. The model has a small thickness which is 0.8% of the model length.

A completely mapped-pixelated mesh was used in this study. The geometry was meshed using quadratic elements (Fig. 6) which give the opportunity to apply periodic boundary condition more accurately. The problem of this method is that the grain boundary between ferrite and martensite (red grains in Fig. 6) is not completely straight line. In order to mesh the real microstructure and to simulate the martensite phase of the material in a good accuracy, a fine mesh resolution (at least 250×250 element on a side) is required (Fig 6a).

In order to do the mesh study, a random microstructure was also produced and meshed by different resolutions. Fig. 6b shows the coarse mesh resolution for the random microstructure. It is obvious that as the mesh resolution increases the boundary of ferrite and martensite grains will be simulated by a better accuracy. The effect of this matter is reported in our mesh study in section 4.2.

## **4. Result and Discussions**

### **4.1. Justification of material parameters**

For the ferrite phase, the parameters of crystal plasticity constitutive law for two slip systems with an overall number of 24 slip planes were adopted to fit the predicted stress strain curve. These parameters are tabulated in Table 1. Fig 8 compares the simulated behavior of the single crystal plasticity model with prediction of the pure ferrite phase behavior using the Rodriguez model. The resulting stress strain curve for DP 800 and its comparison with experimental data is depicted in Fig 9.

### **4.2. Mesh study**

Mesh-size dependency is a well known difficulty in modeling localization problems with finite element analyses due to the non-convergence of solutions with increased refinement of finite element meshing.

In this subsection, we analyze the mesh dependency of our micromechanical analyses with three different meshes. Some implications on mesh quality will also be discussed. The real microstructure could not be used in this study because a certain resolution of mesh was needed to have acceptable similarity between model and SEM pictures. Therefore a random microstructure of 25% martensite content was produced and meshed in three resolutions. The resolutions were the  $100 \times 100 \times 2$ ,  $200 \times 200 \times 2$  and  $400 \times 400 \times 2$  (Numbers refer to elements on each side). The results of this study can be observed in Fig 10 and 11.

Figure 10 d-f shows the field of deformation for the localized field for different resolution of elements. It can be observed that the deformation localization is not affected significantly by element resolution and the location of shear localization is predicted is nearly the same in all models. On the other hand the stress distribution is not the same in different models. Figs 10 g-i shows the distribution of Mises stress in three models. It can be well observed that lower

resolution of mesh causes stress concentration in martensite phase which can be explained as the effect of ferrite-martensite boundary roughness.

The stress strain curve for different mesh resolutions and comparison with experiment is depicted in Fig 11. It can be observed that due to stress localization in martensite phase, higher homogenized value of stress is observed in the model. Refining the mesh leads to a convergence of the results to the experimental values. To study the real microstructure, a mesh resolution of  $250 \times 250$  elements is assumed to be sufficient. This was the minimum resolution which was required to mesh the model of real microstructure.

#### **4.3. Localization and failure initiation for real microstructure and random texture**

Random texture was assigned to the real microstructure which was produced in Fig 5 and then tensile loading was applied to that. The deformed shape in Fig 12a shows the new condition of grain boundaries. A macroscopic engineering strain of 0.40 was applied in this numerical study. This strain value is twice as high as the global fracture strain (see Fig 1), but the local strain in the necked area of the specimen is much more. The true strain at the central point of specimen was calculated using to the reduced area in the neck region. It comes out that the true strain in the central point is 0.15, 0.31, and 0.49 for specimen of diffuse necking, specimen of localized necking, and failed specimen respectively. The simulation models strain of 0.40 which consider state of specimen right before failure.

The stress/ shear strain concentration is an indicator of void initiation in simulation. In this subsection the points of localization would be investigated in more details. Fig 12b shows the mises stress and Fig 12c shows the shear strain. It can be observed that the points of localization for mises stress and shear strain are the same. The sharp ends of martensite grains and more severely between two sharp ends of martensite grains are points of stress/shear strain localization in the simulation. These points are shown by circles in Fig 12c and also Fig 12d. Fig 12d shows the internal pressure in the microstructure. It can be observed that at the

points of stress/shear strain localization (shown by circles in Fig 12c) the internal pressure is negative. Negative internal pressure in tensile loading is an indicator of void initiation in microstructure.

The same pattern can be observed in experiments. The experimental results in Fig 13 shows that the initiation of voids happen mainly at sharp end of martensite grains and in Ferrite/Ferrite grain boundary. It is noteworthy that these voids initiate and grow parallel to the tensile direction. Therefore, they cannot cause the final failure solely.

There are also other points of localization which seem to act like voids in final failure. In these points (shown by arrows in Fig 12c), the ferrite matrix deforms severely due to relative displacement of martensite grains. The process, which was named as shear localization by some authors (Sun (2009a, 2009b)), is investigated in more detail in the next part of this work.

Fig 14 shows the deformation history of several grains. The location of these grains is shown by rectangle in Fig 12a. In Fig 14a-d, the martensite grains are shown by red colours and relative displacement of the 4 martensite grains, indicated by numbers in Fig 14a, is a matter of interest. While Fig 14a shows undeformed shape, Fig 14b, c, d show the deformed shape in strain of 13%, 26% and 40% respectively. Fig 14e, f show the shear strain stress counters in strain of 40%. Fig 14e, f show that the main localization happens due to relative displacement of martensite 1, 3 and martensite 2, 4.

The process of failure initiation can be explained in this way that the relative deformation which has a shear pattern causes a high localized deformation. These localized points are not voids but they are severely deformed and can be considered as sites of failure initiation in microstructure.

Figs 14 g-i show quantitative description about deformation localization process in the ferrite matrix between two martensite grains. Normally it is expected that during tension in x

direction the absolute distance between martensite grains increases in the X direction and decrease in Y direction. For example the absolute distance between grains 1 and 2 shows a continuous increase in Fig 14g. However for some pairs of martensite grains this pattern may differ. For example, the distance between grains 1 and 3 decreases at the beginning ( $\epsilon=0-0.2$ ), but at some point ( $\epsilon=0.2$ ) there is no change in distance between these two grains. Actually these two grains rotate relative to each other after  $\epsilon=0.2$  and the ferrite matrix in between undergoes a severe deformation. As a result the ferrite grain in between yielded and thus the region of ferrite matrix cannot any longer bear the load and is ready for rupture. The same effect occurred between grains 2 and 4.

Fig 15a, b shows these kinds of voids for the failed part. They are not present in the tensile specimens which were interrupted before failure. It seems that their formation happens like a rupture in the final stage of failure. Perhaps the severely deformed regions suddenly separate from each other. Fig 15c shows that on the failure surface of material such patterns occur quite often.

Fig 14e also provides insight about the mechanism of failure. Position A shows the regions that deform severely and are ready for rupture. Position B is expected to be the voids that take place between two ferrite grains in the neighbourhood of a sharp martensite grain. Position C is the shear lines that go through grain and separate the grain into two parts. It is anticipated that A, B, C join together at the end and form the failure line if it was a real microstructure.

Putting experimental and numerical investigations beside each other, it can be concluded that the interaction of ferrite matrix and martensite reinforcement has a rather complicated pattern. Martensite matrix is the harder phase. It has less deformation than ferrite but the displacement of martensite is determined by the ferrite matrix. Martensite location changes because the neighbouring ferrites deform much more. In this study two sources of failure initiation were identified:

1. The martensite reinforcement deforms less than the neighbouring ferrite matrix. Therefore, at the sharp ends of martensite grains negative pressure can be observed. At these points voids are expected to initiate.
2. Some martensite reinforcements have a large relative displacement in microstructure. The reason was explained before. Due to this displacement the relative position of martensite grains change and the ferrite matrix experience severe deformation at some points. These points are also incapable of load bearing in final stages and have a rupture like failure in final stages of tensile test.

#### **4.4. Simulation results for real microstructure and real texture**

In this last part the real texture was assigned to the microstructure. The idea is to get some insight about how the texture effects shear localization in the microstructure. The results for real texture are shown in Fig 16 and the results using random texture are in Fig 12. When the real texture is assigned to the model, the shear banding is more intense as depicted in Figs 16a, b. This phenomenon was also previously observed through simulations by other researchers (Delannay (2008), Dao (2001), Kuroda (2007)). However, their simulations were for single phase material while in this work the simulations were carried out for dual phase material. It seems that, relative to random texture, the real texture causes the tendency to shear localization in the material and the joint of shear bands together and creation of failure line. One can explain this phenomenon in the following way. As the real rolling texture is assigned to the microstructure, it was observed that the probability of having similar orientation by grains increases relative to a uniformly distributed random texture. Such an observation was also reported in Dao (2001). Due to this fact, the shear band may take place in locations that are near to each other and thus create a failure lines. Also the neighboring grains which have similar orientation may deform in the same direction and this allows the easier creation of shear band inside one of the grains.



## **Conclusions**

Experimental and numerical observation was carried out to investigate the failure process in dual phase steels. The results showed that the failure pattern is not severely deviated from classical ductile failure. But it was observed that relative deformation of martensite grains causes high deformation localization in ferrite matrix and it play an important role in final failure of material.

## **References**

Ahmed, E., Tanvir, M., Kanwar, L.A., Akhter, J.I., 2000. Effect of Microvoid Formation on the Tensile Properties of Dual-Phase Steel. *Journal of Materials Engineering and Performance* (9), 306–310.

Al-Abbasi, F.M., Nemes, J.A., 2007. Characterizing DP-steels using micromechanical modeling of cells. *Computational Materials Science* (39), 402–415.

Anand, L., Kalidindi, S.R., 1994. The process of shear band formation in plane strain compression of fcc metals: Effects of crystallographic texture, *Mechanics of Materials* (17), 223-243.

Avramovic-Cingara, G., Ososkov, Y., Jain, M.K., Wilkinson, D.S.; (2009a). Effect of martensite distribution on damage behaviour in DP600 dual phase steels; *Materials Science and Engineering A* (516) 7-16.

Avramovic-Cingara, G., Saleh, Ch.A.R., Jain, M.K., Wilkinson, D.S.; (2009b). Void Nucleation and Growth in Dual-Phase Steel 600 during Uniaxial Tensile Testing; *Metallurgical and Materials Transactions A* (40) 3117-3127

Asaro, R.J., 1983a. Crystal plasticity. *J. Appl. Mech.* (50), 921-934.

Asaro, R.J., 1983b. Micromechanics of Crystals and Polycrystals. *Adv. Appl. Mech.* (23), 1-115.

Barbe, F., Decker, L., Jeulin, D., Cailletaud, G., 2001. Intergranular and intragranular behavior of polycrystalline aggregates. Part 1: F.E. model. *International Journal of Plasticity* (17), 513-536.

Balliger, N.K., 1982. *Advances in the Physical Metallurgy and Applications of Steels*, Book 284. The Metals Society, London.

Bieler, T.R., Eisenlohr, P., Roters, F., Kumar, D., Mason, D.E., Crimp, M.A., Raabe, D., 2009. The role of heterogeneous deformation on damage nucleation at grain boundaries in single phase metals. *International Journal of Plasticity* (25), 1655-1683.

Bouaziz, O., Embury, J.D., 2007. Microstructural design for advanced structural steels. *Mater. Sci. Forum* (539), 42-50

Calcagnotto, M., Ponge, D., Adachi, Y., Raabe, D., (2009). Effect of Grain Refinement on Strength and Ductility in Dual-Phase Steels, *Proceedings of the 2nd International Symposium on Steel Science (ISSS 2009)*, Kyoto, Japan.

Dao, M., Li, M., 2001. A micromechanics study on strain-localization-induced fracture initiation in bending using crystal plasticity models, *Philosophical Magazine A* (81), 1997–2020.

Delannay, L., Kanjarla, A.K., Melchior, M.A., Signorelli, J.W., Van Houtte, P., (2008) Cpfem investigation of the effect of grain shape on the planar anisotropy and the shear banding of textured metal sheets, In: *Applications of Texture Analysis (Proc. Icotom, CMU Pittsburg, June2008)* Ed. A.D. Rolett, *Ceramic Transactions* (201) 745-756.

Diard, O., Leclercq, S., Rousselier, G., Cailletaud, G., (2005). Evaluation of finite element based analysis of 3D multicrystalline aggregates plasticity: Application to crystal plasticity model identification and the study of stress and strain fields near grain boundaries. *International Journal of Plasticity* (21), 691–722.

Eisenlohr P., Roters F. (2008). Selecting a set of discrete orientations for accurate texture reconstruction, *Computational Materials Science* (42) 670–678

Erdogan, M., 2002. The effect of new ferrite content on the tensile fracture behaviour of dual phase steels. *J. Mater. Sci.* (37), 3623-3630.

Gerbase, J., Embury, J.D., Hobbs, R.M., 1979. In Kot, R.A., Morris, J.W., *Structure and Properties of Dual- Phase Steels*. AIME, New York, NY, 118–143.

Gladman, T., 1997. *The Physical Metallurgy of Microalloyed Steels*, The Institute of Materials, The University Press, Cambridge, London.

Gurson, A. L., 1977. Theory of Ductile Rupture by Void Nucleation and Growth: Part I- Yield Criteria and Flow Rules for Porous Ductile Media. *J. Eng. Mat. Techn.* (99), 2-15.

Hill, R., Rice, J.R., 1972. Constitutive analysis of elastic-plastic crystals at arbitrary strain. *J. Mech. Phys. Solids* (20), 401-413.

Huang, Y., 1991. A user-material subroutine incorporating single crystal plasticity in the ABAQUS Finite Element Program. Mech. Report 178, Division of Applied Sciences, Harvard University, Cambridge, MA.

Kang, S., Kwon, H., 1987. Fracture Behavior of Intercritically Treated Complex Structure in Medium-Carbon 6 Ni Steel. *Metallurgical Transactions A* (18), 1587–1592.

Kang, J., Ososkov, Y., Embury, J.D., Wilkinson, D.S., 2007. Digital image correlation studies for microscopic strain distribution and damage in dual phase steels. *Scripta Mater* (56), 999-1002

Kim, N.J., Thomas, G., 1981. Effects of morphology on the mechanical behavior of a dual phase Fe/2Si/0.1C steel. *Metallurgical Transactions A* (12), 483-489

K-Kanjarla, A., Van Houtte, P., Delannay, L, 2010. Assessment of plastic heterogeneity in grain interaction models using crystal plasticity finite element method, *International Journal of Plasticity* (26) 1220-1233

Koo, J.Y., Thomas, G., 1977. Design of Duplex Low Carbon Steels for Improved Strength. In: Davenport, A.T., Weight Applications. *Formable HSLA and Dual Phase Steels*. AIME, New York. 40–55,

Korzekwa, D.A., Lawson, R.D., Matlock, D.K., Krauss, G., 1980. A Consideration of Models Describing the Strength and Ductility of Dual-Phase Steels. *Scripta Metallurgica* (14), 1023–1028.

Kosco, J.B., Koss, D.A., 1993. Ductile fracture of mechanically alloyed iron-yttria alloys. *Metall. Trans. A* (24), 681-687.

Kumar, A., Singh, S.B., Ray, K.K., 2008. Influence of bainite/martensite-content on the tensile properties of low carbon dual-phase steels, *Mater. Sci. and Eng. A* (474), 270-282

Kuroda, M., Tvergaard, V., (2007). Effects of texture on shear band formation in plane strain tension/compression and bending, *Int. J. Plast.* (23), 244-72

Kwon, D., 1988. Interfacial decohesion around spheroidal carbide particles. *Scripta Metall* (22), 1161-1164.

Lee, H.S., Hwang, B., Lee, S., Lee, C.G., Kim, S.J., 2004. Effects of martensite morphology and tempering on dynamic deformation behavior of dual-phase steels. *Metall. Mater. Trans. A* (35), 2371-2382.

LeRoy, G., Embury, J.D., Edwards, G., Ashby, M.F., 1981. A model of ductile fracture based on the nucleation and growth of voids. *Acta Metall.* (23), 1509-1522.

Ma, A., Roters, F., Raabe, D., 2006a. A dislocation density based constitutive model for crystal plasticity FEM including geometrically necessary dislocations. *Acta Materialia* 54 (8), 2169–2179.

Ma, A., Roters, F., Raabe, D., 2006b. On the consideration of interactions between dislocations and grain boundaries in crystal plasticity finite element modeling – theory, experiments, and simulations. *Acta Materialia* 54 (8), 2181–2194.

Maire, E., Bouaziz, O., Michiel, M. D., Verdu, C., 2008, Initiation and growth of damage in a dual-phase steel observed by X-ray microtomography. *Acta Materialia* (18), 4954-4964.

Marketz, W.T., Fisher, F.D., Clemens, H., 2003. Deformation mechanisms in TiAl intermetallics – experiments and modeling. *Int. J. Plasticity* (19), 281–321.

McVeigh, C., Vernerey, F., Liu, W.K., Moran, B., Olson, G., 2007. An interactive micro-void shear localization mechanism in high strength steels. *Journal of the Mechanics and Physics of Solids* (55), 225–244.

Nakamachi, E., Hiraiwa, K., Morimoto, H. and Harimoto, M., 2000. Elastic/crystalline viscoplastic finite element analyses of single- and poly-crystal sheet deformations and their experimental verification. *Int. J. Plasticity* (16), 1419–1441.

Nam, W.J., Bae, C.M., 1999. Microstructure Evolution and its Relation to Mechanical Properties in a Drawn Dual-Phase Steel. *Journal of Material Science* (34), 5661–5668.

Orsini, C., Zikry, M.A., 2001. Void growth and interaction in crystalline materials. *International Journal of Plasticity* (17), 1393–1417.

Osipov, N., Gourgues-Lorenzon, A.-F., Marini, B., Mounoury, V., Nguyen, F., Cailletau, G., 2008. FE modelling of bainitic steels using crystal plasticity, *Philosophical Magazine* (88), 3757–3777

Poruks, P., Yakubtsov, I., Boyd, J.D., 2006. Martensite–ferrite interface strength in a low-carbon bainitic steel. *Scripta Materialia* (54), 41-45.

Prakash, A., Weygand, S.M., Riedel, H., 2009. Modeling the evolution of texture and grain shape in Mg alloy AZ31 using the crystal plasticity finite element method. *Computational Materials Science* (45), 744-750.

Qiu, H., Mori, H., Enoki, M., Teruo, K., 1999. Evaluation of ductile fracture of structural steels by microvoid model. *ISIJ Int.* (39), 358-364.

Rashid, M.S., 1977. GM 980X-A Unique High Strength Sheet Steel with Superior Formability. Paper 760206. Soc. Auto. Eng. Cong., Detroit, 938–949.

Rashid, M.S., Cprek, E.B., 1978. Relationship Between Microstructure and Formability in Two High-Strength, Low-Alloy Steels, *Formability Topics – Metallic Materials*, ASTM STP 647, American Society for Testing and Materials, Philadelphia, PA, 174–190.

Rice, J. R., Tracey, D. M., 1969. On the ductile enlargement of voids in triaxial stress fields. *J. Mech. and Phys. Solids* (17), 201-217

Rice, J.R., 1971. Inelastic constitutive relations for solids: An internal-variable theory and its application to metal plasticity. *J. Mech. Phys. Solids* (19), 433-455.

Riedel, H., 1992. Fracture mechanisms, Fraunhofer-Inst. für Werkstoffmechanik

Rodriguez, R., Gutierrez, I., 2004. Proc. TMP'2004, Ed. M. Lamberigts, Verlag Stahleisen GMBH, Düsseldorf, 356.

Schmidt, E., 1931. Über die Schubverfestigung von Einkristallen bei plastischer Deformation. Z. Phys. (40), 54–60.

Shen, H.P., Lei, T.C., Liu, J.Z., 1986. Microscopic deformation behavior of martensitic-ferritic dual phase steels. Mater Sci and Tech (2), 28-33

Speich, G.R., Miller, R.L., 1979. In Kot, R.A., Morris, J.W., Structure and Properties of Dual-Phase Steels. TMS-AIME, New York. 145–182.

Spitzig, W.A., Smelser, R.E., Richmond, O., 1988. The evolution of damage and fracture in iron compacts with various initial porosities. Acta Metall. (36), 1201-1211.

Suh, D., Kwon, D., Lee, S., Kim, N.J., 1997. Orientation dependence of microfracture behavior in a dual-phase high-strength low-alloy steel. Metall. Trans. A (28), 504-509.

Sun, S., Pugh, M., 2002. Properties of thermo chemically processed dual-phase steels containing fibrous martensite. Materials Science & Engineering (335), 298–308.

Sun, X., Choi, K.S., Liu, W.N., Khaleel, M.A., 2009a. Predicting failure modes and ductility of dual phase steels using plastic strain localization. Int. J. Plasticity (25), 1888-1909.

Sun, X., Choi, K.S., Soulami, A., Liu, W.N., Khaleel, M.A., 2009b. On key factors influencing ductile fractures of dual phase (DP) steels. Materials Science and Engineering A (526) 140-149.

Steinbrunner, D.L., Krauss, G., 1988. Void formation during tensile testing of dual phase steels. Metallurgical Transactions A (9), 579–589.

Szewczyk, A.F., Gurland, J., 1982. A Study of The Deformation and Fracture of a Dual-Phase Steel. *Metallurgical Transactions A* (13), 1821–1826.

Tasan, C.C., Hoefnagels, J.P.M., Geers, M.G.D., 2009. A critical assessment of indentation-based ductile damage quantification. *Acta Materialia* (57), 4957-4966.

Tomota, Y., Tamura, I., 1982. Mechanical behavior of steels consisting of two ductile phases. *Transactions of the Iron and Steel Institute of Japan* (22), 665-677.

Uthaisangsuk, V., Prahl, U., Münstermann, S., Bleck, W., (2008). Experimental and numerical failure criterion for formability prediction in sheet metal forming, *Computational Materials Science*, (43), 43-50

Uthaisangsuk, V., Prahl, U., Bleck, W., (2009). Characterisation of formability behaviour of multiphase steels by micromechanical modeling, *International Journal of Fracture*, (157), 55-59

Zaafarani, N., Raabe, D., Singh, R.N., Roters, F., Zaefferer, S., 2006. Three-dimensional investigation of the texture and microstructure below a nanoindent in a Cu single crystal using 3D EBSD and crystal plasticity finite element simulations. *Acta Materialia* 54 (7), 1863–1876.



Figures Caption:

**Figure 1:** Engineering stress strain curve of DP800

**Figure2:** Microstructure of the DP800 steel in two different magnifications.

**Figure 3.** Investigation of failure process in tensile specimen for dual phase steel at different strains: diffuse necking (first row: a, b, c ,d); localized necking (second row: e, f, g, h) and failure (third row: i, j, k, l) [It comes out that the true strain in the central point is 0.15, 0.31, and 0.49 for specimen of diffuse necking, specimen of localized necking, and failed specimen respectively]

- **Fig 3-a.** Diffuse necking ( $\epsilon_{\text{eng}} \approx 0.12$ ) →
- **Fig 3-e.** Localized necking( $\epsilon_{\text{eng}} \approx 0.17$ )→
- **Fig 3-i.** Failure ( $\epsilon_{\text{eng}} \approx 0.20$ )→

**Figure 4:** The fracture morphology show homogeneous distribution of dimples and small number of inclusions are present in the voids

**Figure 5:** generation of micromechanical model for DP800 steel

- **Fig 5-a.** SEM picture
- **Fig 5-b.** binarised microstructure
- **Fig 5-c.** texture
- **Fig 5-d.** crystal plasticity model

**Figure 6:** Mesh of the model (a)fine mesh for real microstructure and (b) coarse model for the randomly produced microstructure (This figure shows the mesh for a part of the model)

**Figure 7:** stress strain curve for (a) ferrite of 0.02% carbon content and 5 $\mu\text{m}$  grain diameter and (b) martensite of 0.64% carbon content

**Figure 8:** Crystal plasticity model for behaviour of ferrite phase

**Fig 9:** Experimental behaviour and result of simulation for DP800

**Figure 10:** Mesh convergence study for three different discretisations of the finite element mesh. The accumulated plastic strain and the Mises equivalent stress are illustrated for an engineering strain value of 0.15

**Figure 11:** The stress strain curve for the DP steel behaviour in different element resolution; True value(a) and engineering value (b)

**Figure 12:** Deformed shape of grains(a) von Mises equivalent stress(b) accumulated shear plastic deformation (c) and hydrostatic pressure (d)

- *Fig 12-a.* Deformed shape
- *Fig 12-b.* Mises stress
- *Fig 12-c.* Accumulated shear strain
- *Fig 12-d.* internal pressure

**Figure 13:** Points of void initiation in SEM picture of tensile specimen

**Figure 14:** Detailed history of deformation in microstructure (a, b, c, d) as the source of stress/shear strain localization (e, f); and relative distance between the martensite grains (g, h, i) [The distance between martensite grain centers is tracked in g,h,i]

- *Fig 14-a.*  $\epsilon=0\%$
- *Fig 14-b.*  $\epsilon=13\%$
- *Fig 14-c.*  $\epsilon=26\%$
- *Fig 14-d.*  $\epsilon=40\%$
- *Fig 14-e.* Shear strain

- **Fig 14-f.** Mises stress

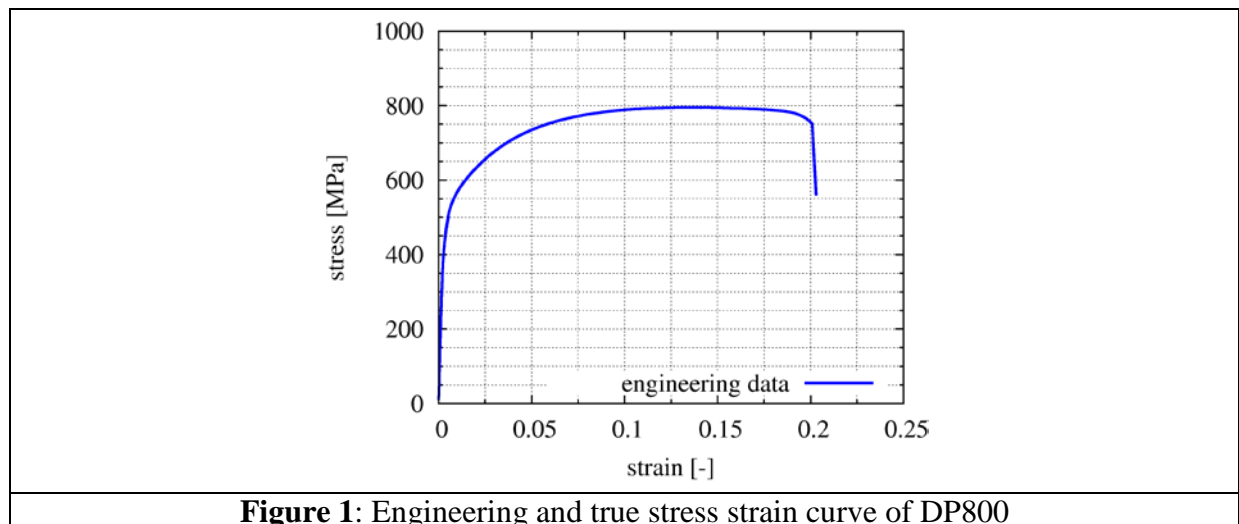
**Figure 15:** Voids which can be observed in the failed part (a, b) and the failure surface (c)

**Figure 16:** von Mises equivalent stress(a) accumulated shear plastic deformation (b) and hydrostatic pressure (c) of model with real texture

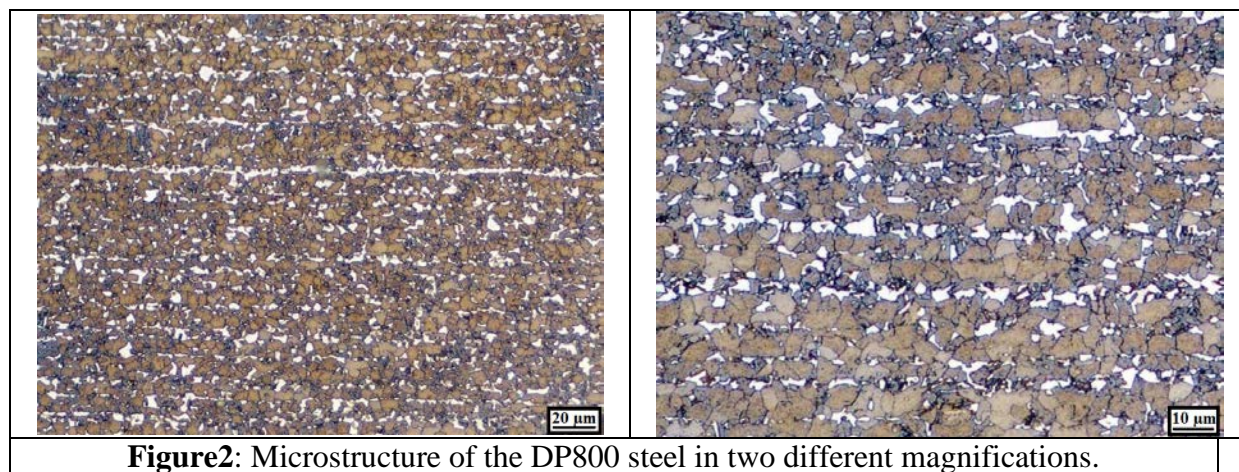
- **Fig 12-a.** Mises stress
- **Fig 12-b.** Accumulated shear strain
- **Fig 12-c.** internal pressure

Table caption

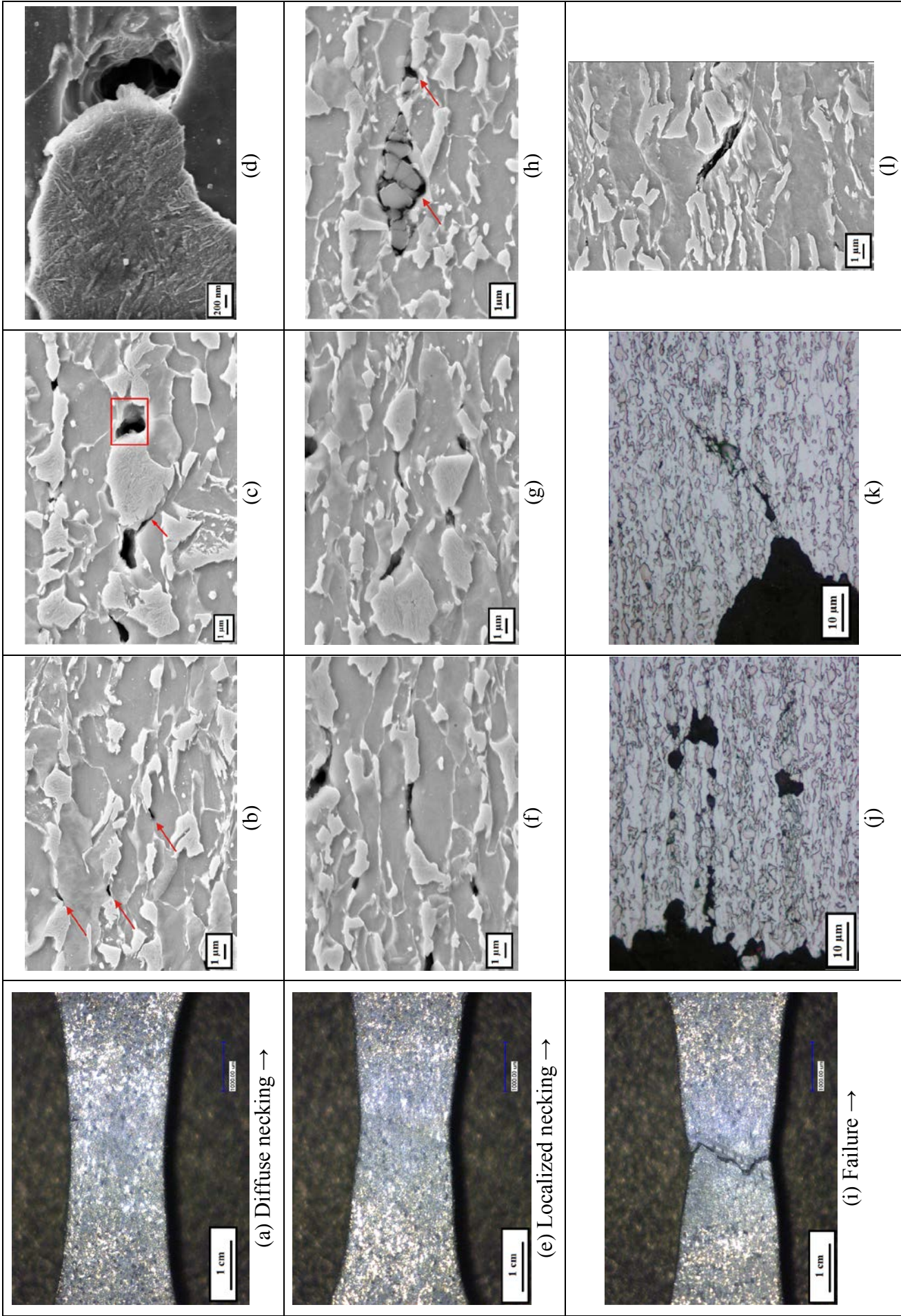
**Table1:** Crystal Plasticity constants for ferrite phase



**Figure 1:** Engineering and true stress strain curve of DP800

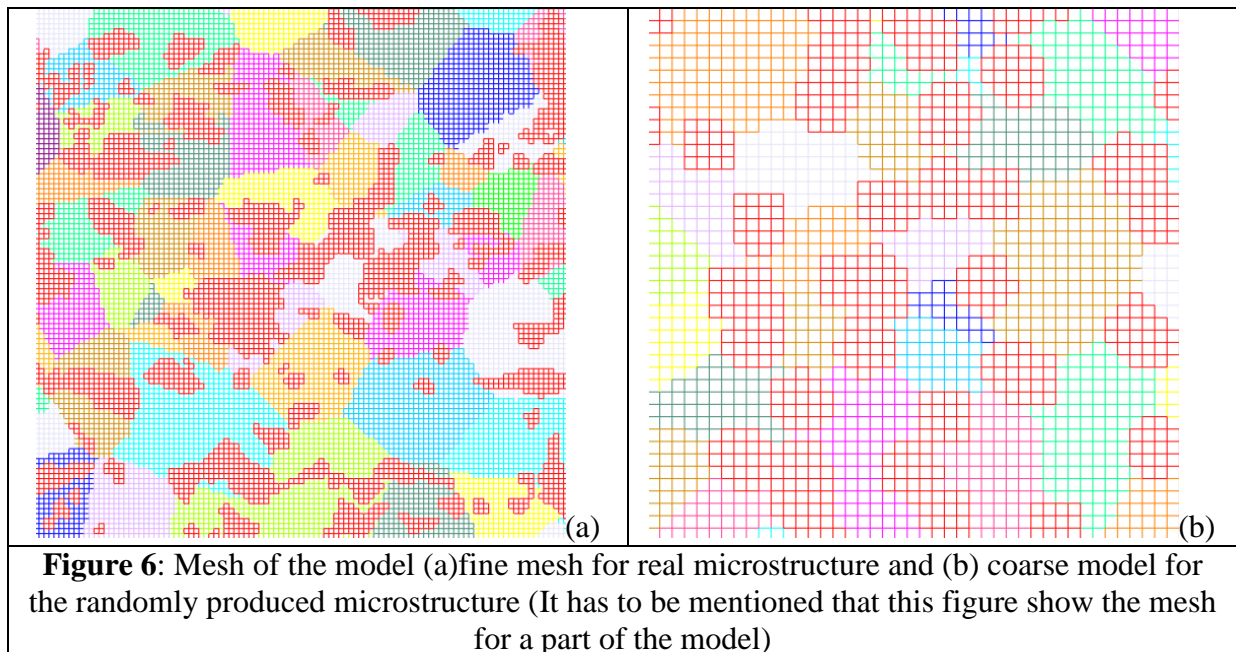
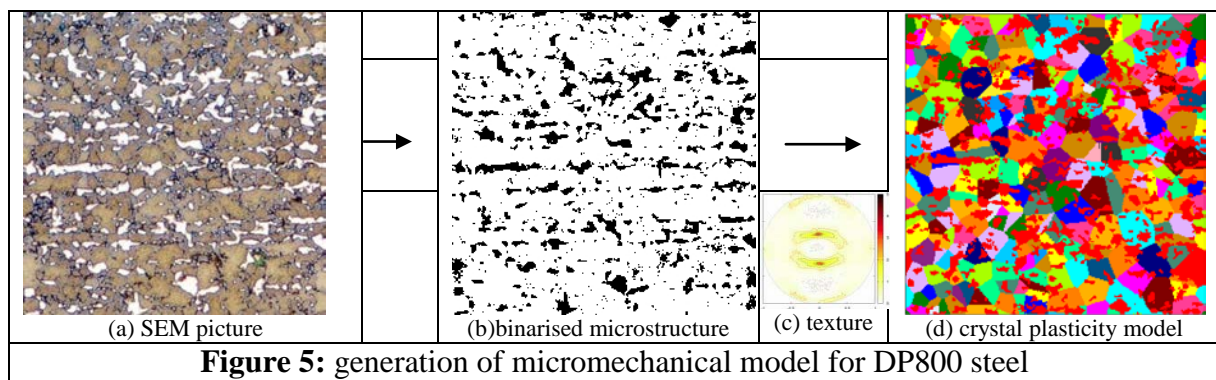
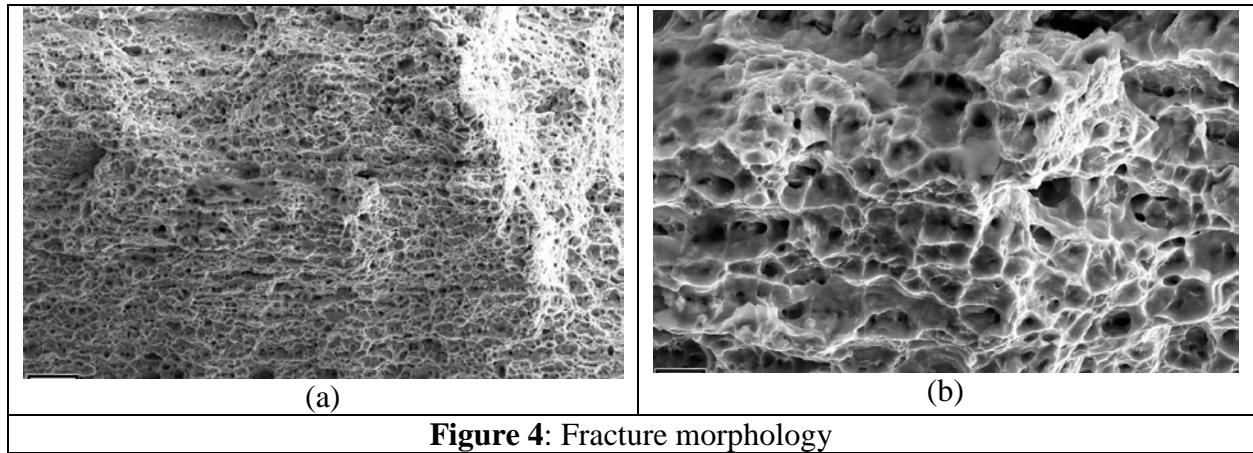


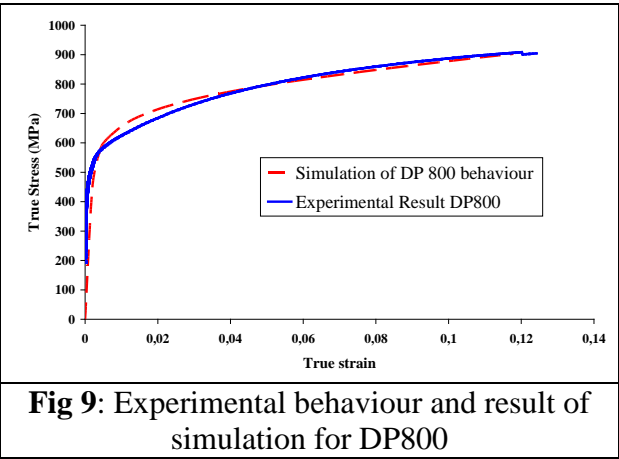
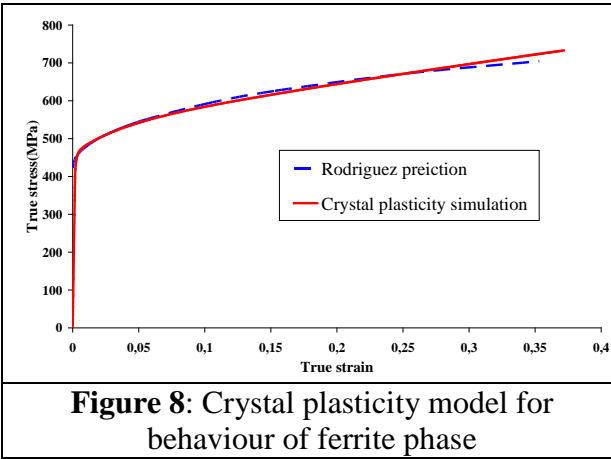
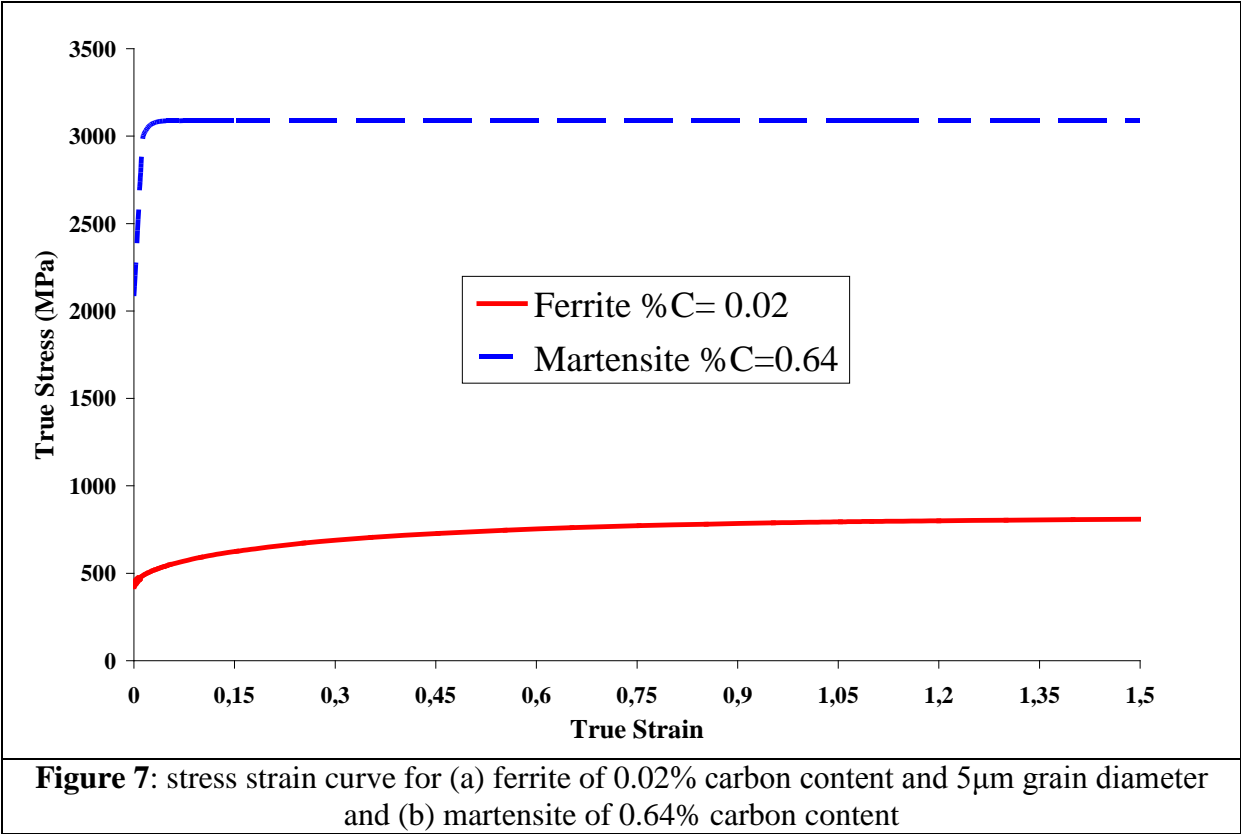
**Figure2:** Microstructure of the DP800 steel in two different magnifications.



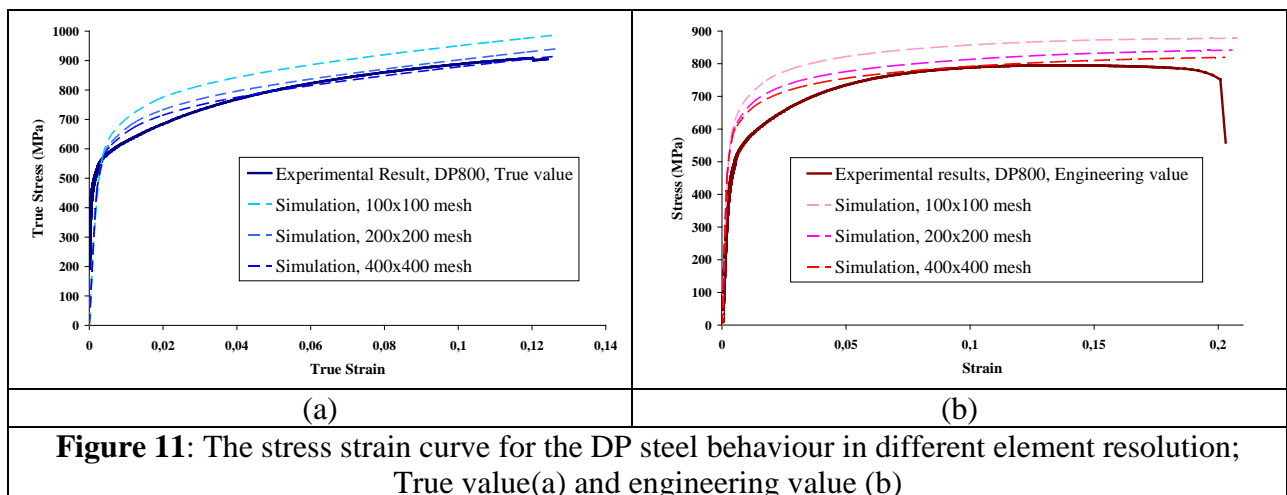
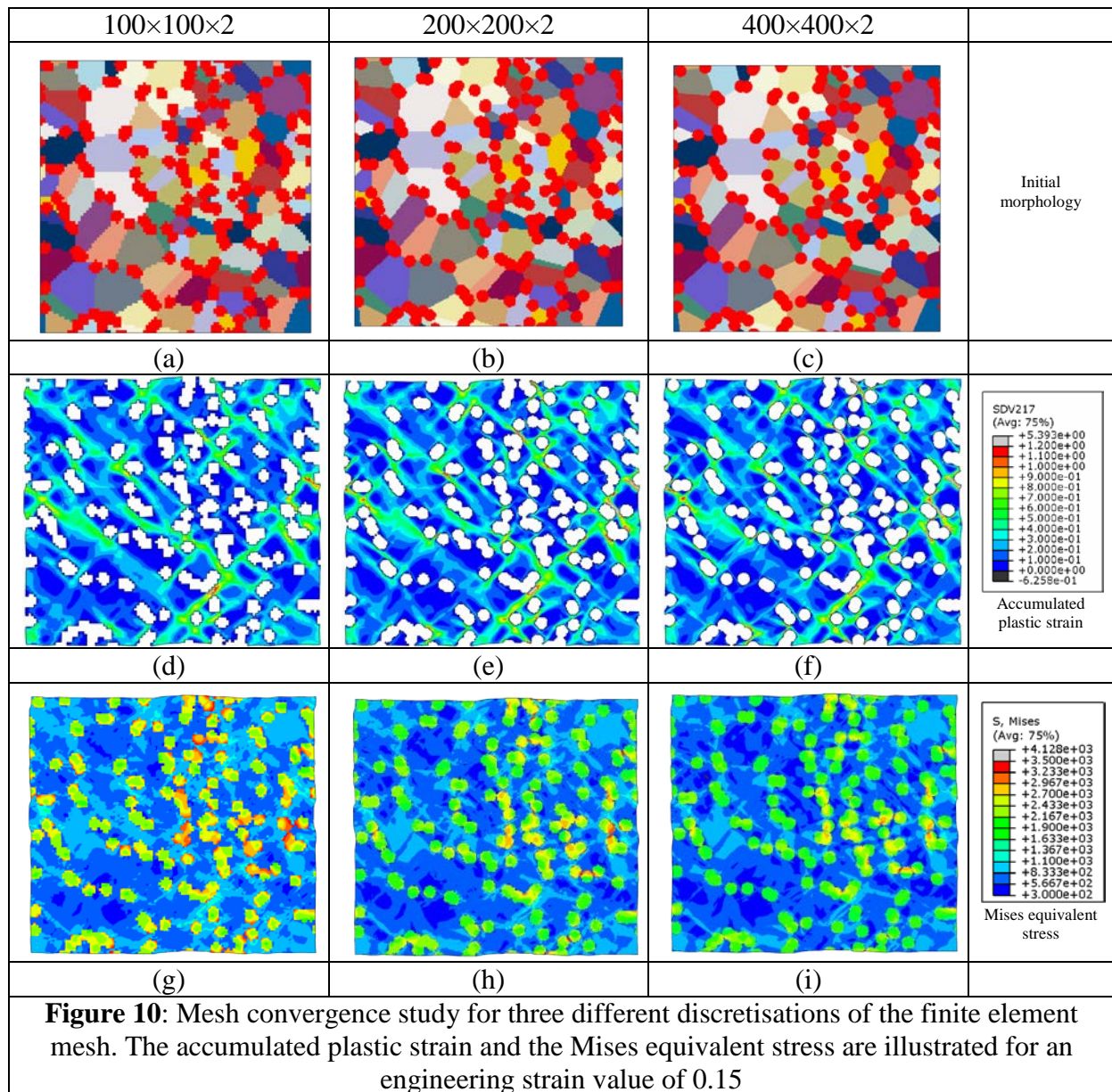
**Figure 3.** Investigation of failure process in tensile specimen for dual phase steel indifferent steps: diffuse necking (first raw: a, b, c, d); localized necking (second raw: e, f, g, h) and failure (third raw: i, j, k, l)



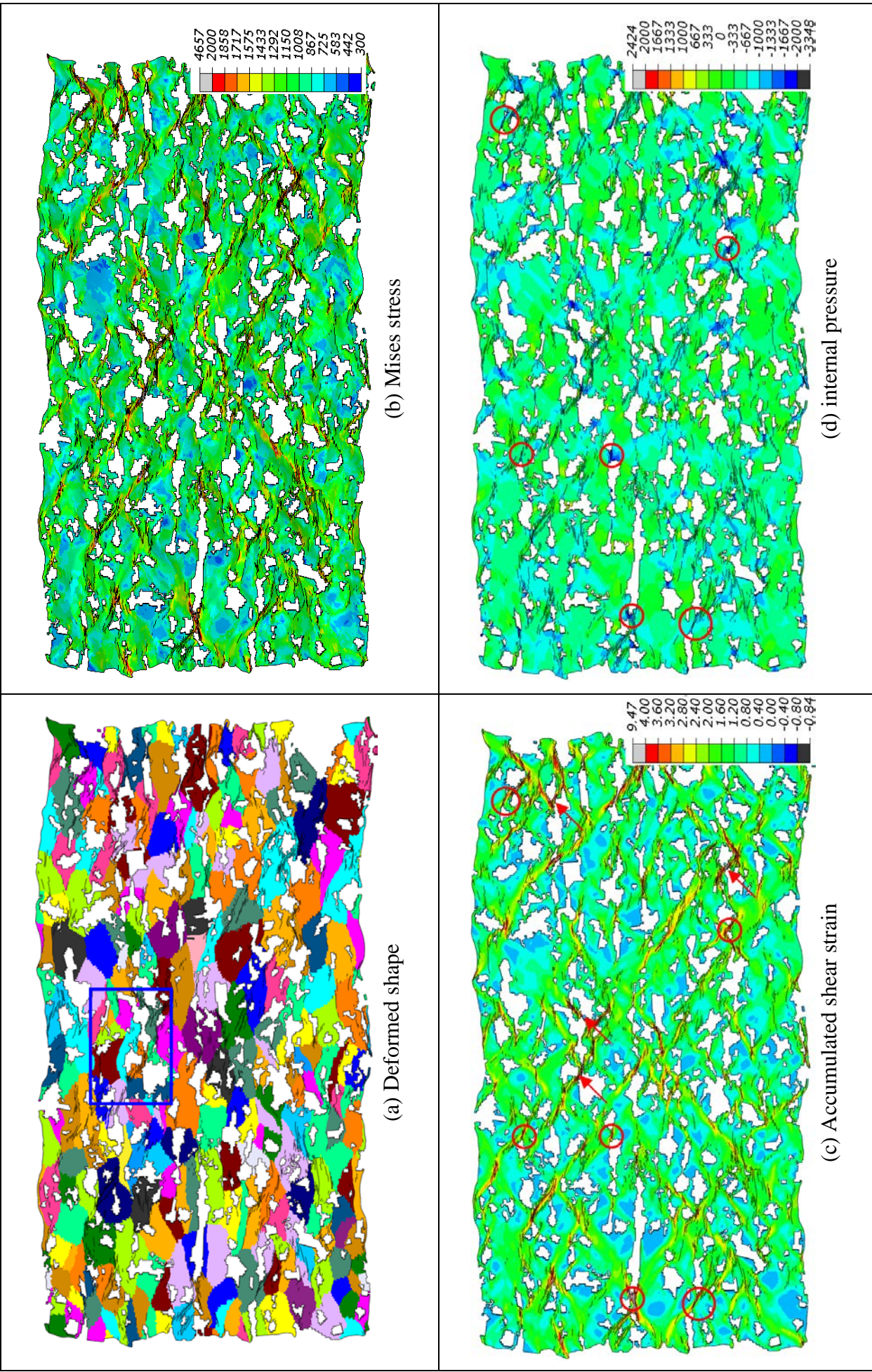




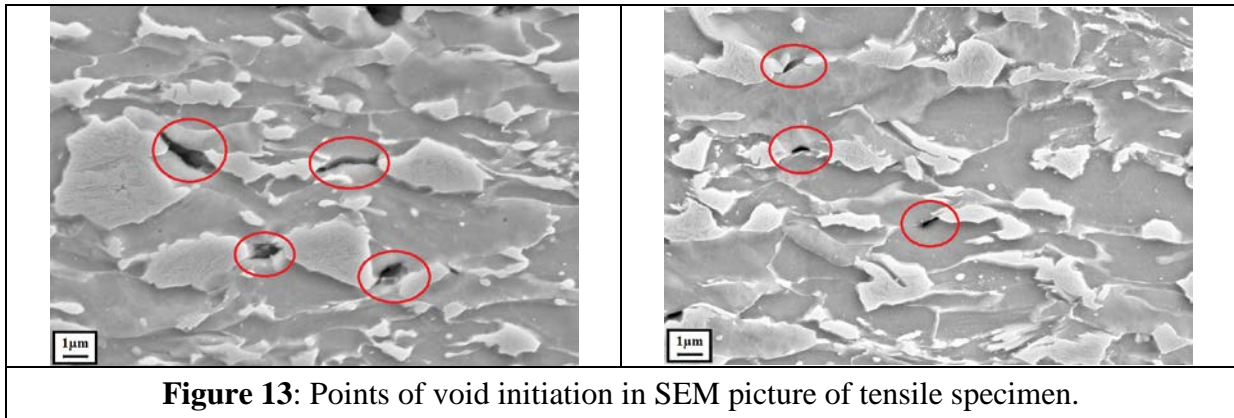
$\mu$ m







**Figure 12:** Deformed shape of grains(a) von Mises equivalent stress(b) accumulated shear plastic deformation (c) and hydrostatic pressure (d)





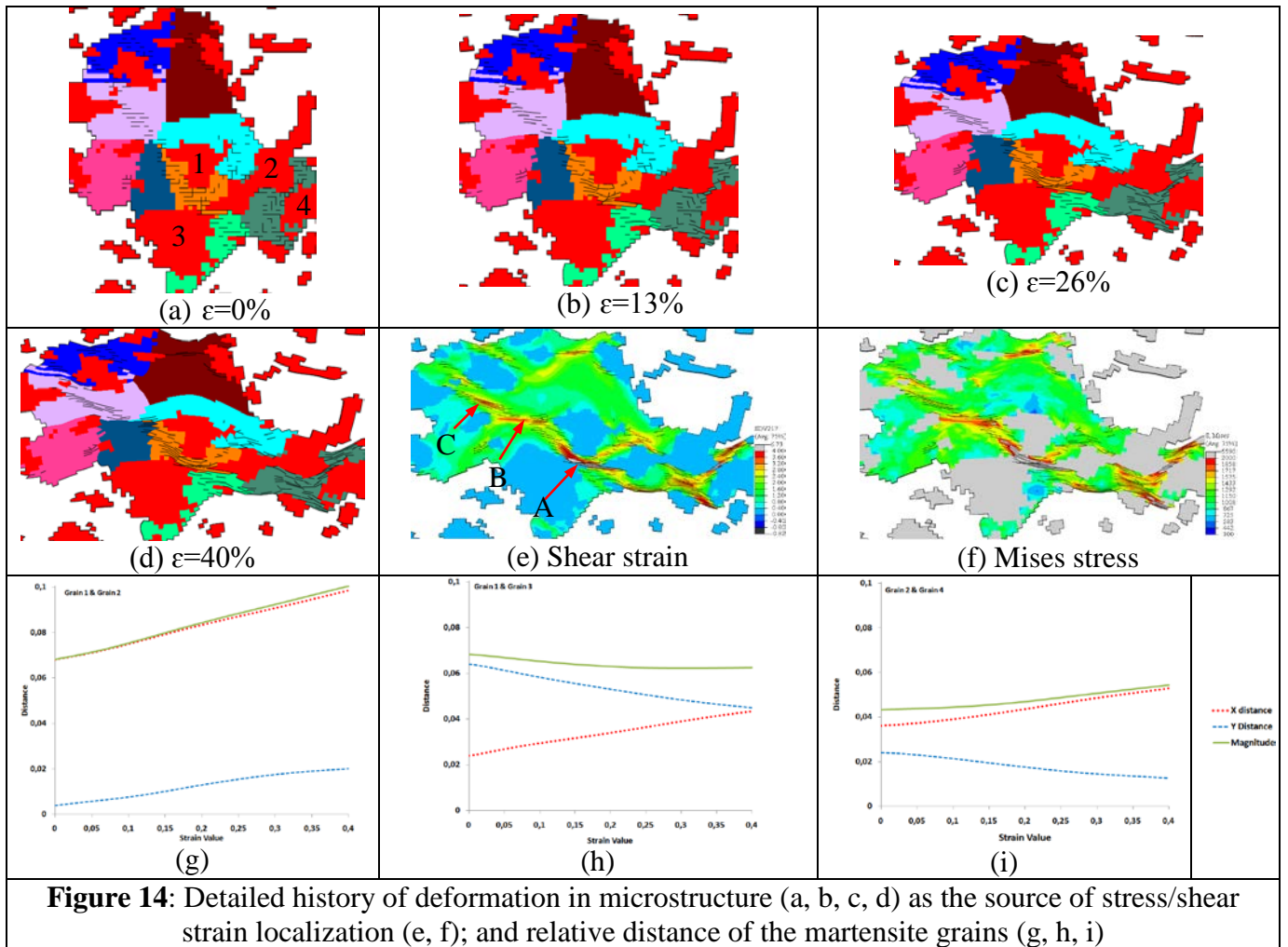


**Figure 14:** Detailed history of deformation in microstructure (a, b, c, d) as the source of stress/shear strain localization (e, f); and relative distance of the martensite grains (g, h, i)

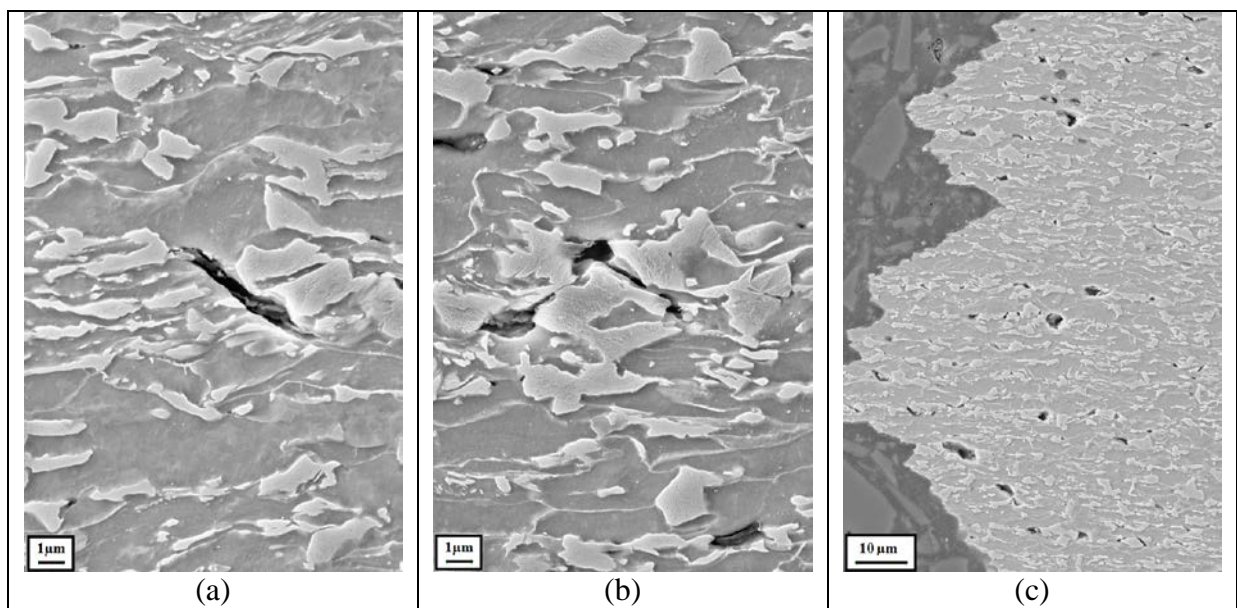
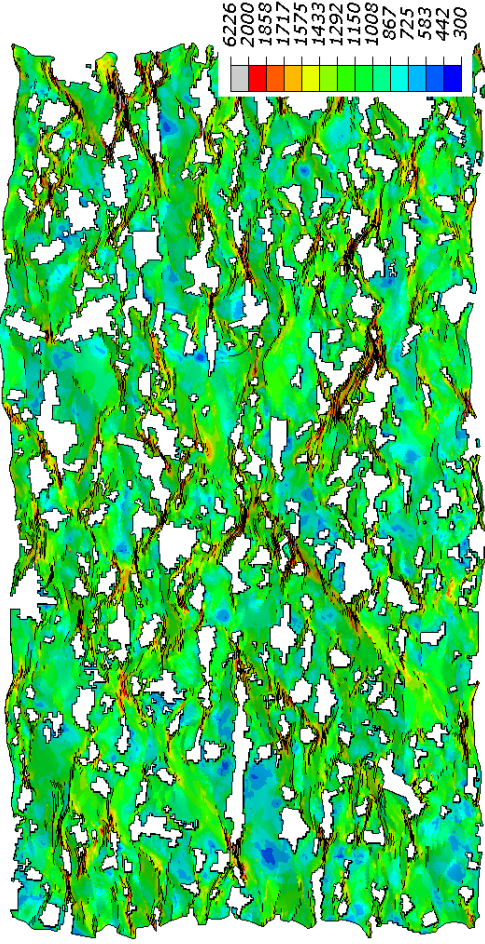
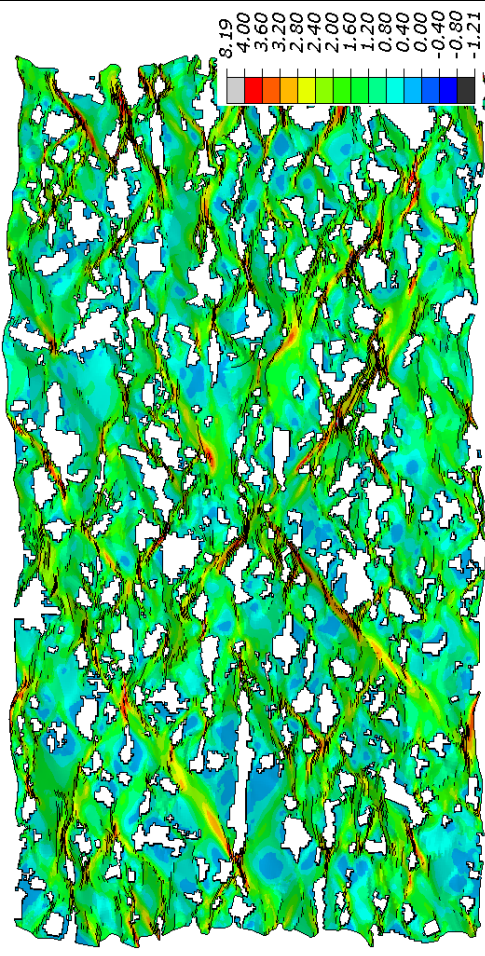


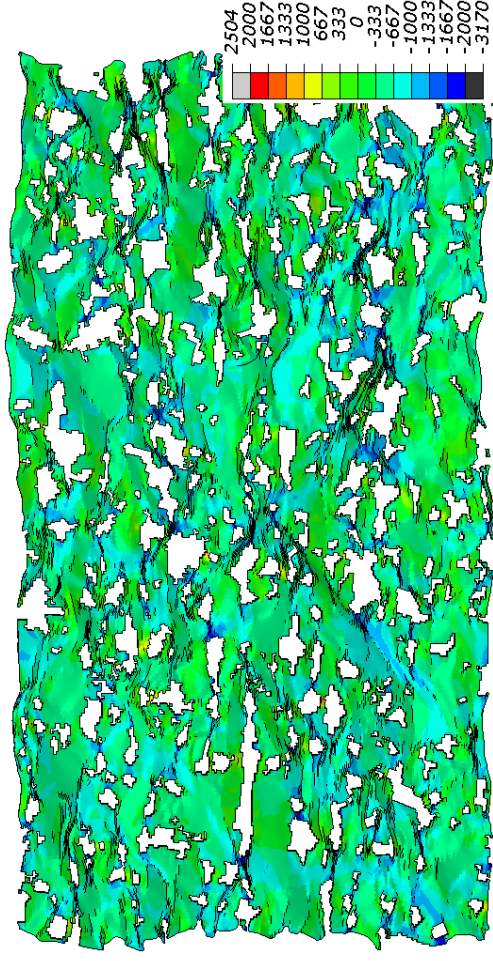
**Figure 15:** Voids which can be observed in the failed part (a, b) and the failure surface (c)



(a) Mises stress



(b) Accumulated shear strain



(c) internal pressure

**Figure 16:** von Mises equivalent stress(a) accumulated shear plastic deformation (b) and hydrostatic pressure (c) of model with real texture

**Table1:** Crystal Plasticity constants for ferrite phase

Slip system	$\tau_0(MPa)$	$\tau_1(MPa)$	$\theta_0(MPa)$	$\theta_1(MPa)$	Single-crystal elastic constants		
					$C_{11}(GPa)$	$C_{12}(GPa)$	$C_{44}(GPa)$
$\{110\}\langle 111\rangle$	198	30	350	83	236	140	116
$\{112\}\langle 111\rangle$	228	35	400	93			